Available online at www.sciencedirect.com
SCIENCE DIRECT®
Journal of Magnetism and Magnetic Materials 300 (2006) e371–e374
Journal of magnetism and magnetic materials
www.elsevier.com/locate/jmmm

Depth selective investigations of magnetic multilayers by X-ray resonant magnetic reflectivity

M.A. Andreeva[a,*], A.G. Smekhova[a], B. Lindgren[b], M. Björck[b], G. Andersson[b]

[a]*Faculty of Physics, M.V. Lomonosov Moscow State University, Leninskie Gory, GSP-2, Moscow 119992, Russia*
[b]*Department of Physics, Faculty of Science and Technology, Uppsala University, Box 530, 751 21 Uppsala, Sweden*

Available online 15 November 2005

Abstract

We have measured and analyzed the X-ray resonant Bragg reflectivity spectra from BCC $[Fe/Co]_n$ superstructure near the $L_{2,3}$ absorption edges of iron. The developed general computer code for the reflectivity calculations from arbitrary anisotropic multilayers allows us to test the different approaches to the treatment of the Bragg reflectivity spectra. We have proved that the observed asymmetry of the spectrum shape at the first-order Bragg peak for the right and left circular polarizations is predominantly caused by the magnetization of the central part of iron layers. The influence of interfaces is almost negligible. The fit of the energy dependence of the integral intensity of the Bragg reflection for the $[Fe_6/Co_6]_{50}$ sample gives the value of the magnetic moment of Fe atoms in the central parts of Fe layers $\sim 2.6\,\mu_B$, that is larger than the volume value.

PACS: 75.70.Cn; 78.70.Ck; 68.35.Ct

Keywords: Magnetic circular reflectivity; Fe/Co superlattice; Magnetic moment; Interface roughness

1. Introduction

Nowadays the X-ray resonant absorption and scattering near the $L_{2,3}$ edges of transition metals is an effective and element specific tool for magnetic material investigations. Every known magneto-optical phenomena (P-, T- and L-MOKE, Faraday rotation, Voigt effect, XMCD, etc.) have been observed with linear or circular polarized X-rays [1,2]. The essential new feature of X-ray magneto-optics is the possibility to combine X-ray resonant spectroscopy with diffraction on a crystal structure or with reflection from multilayers. In such a way we get a space or depth resolution of the method [3].

The interpretation of the resonant spectra of reflectivity is much more complicated than that of the absorption spectra. The effective usage of the X-ray resonant absorption spectra in magnetic investigations is provided by the applicability of the so-called sum rules [4], which make possible the direct determination of the orbital and spin magnetic moments of the resonant atoms from the resonant $L_{2,3}$ or $M_{4,5}$ spectrum shape. The reflectivity spectra possess a high sensitivity to the polarization state of the incident radiation (e.g. large asymmetry of the reflectivity spectra is observed for the right and left circular polarization of X-rays in L-MOKE geometry), but no simple receipts have been developed for the determination of the magnetic moments from reflectivity spectra. For hard X-rays, when the reflectivity is investigated at small glancing angles, the interpretation is simplified and the remarkable results were obtained in Ref. [5] for the depth profile determination of the magnetic moment. For soft X-rays the interpretation of the reflectivity spectra is more complicated.

Here we test the different approaches to determination of the optical and magnetic parameters from the resonant

*Corresponding author. Tel.: +7 275 11157; fax: +7 095 9328820.
E-mail address: marina@ttk.ru (M.A. Andreeva).

0304-8853/$ - see front matter © 2005 Elsevier B.V. All rights reserved.
doi:10.1016/j.jmmm.2005.10.131

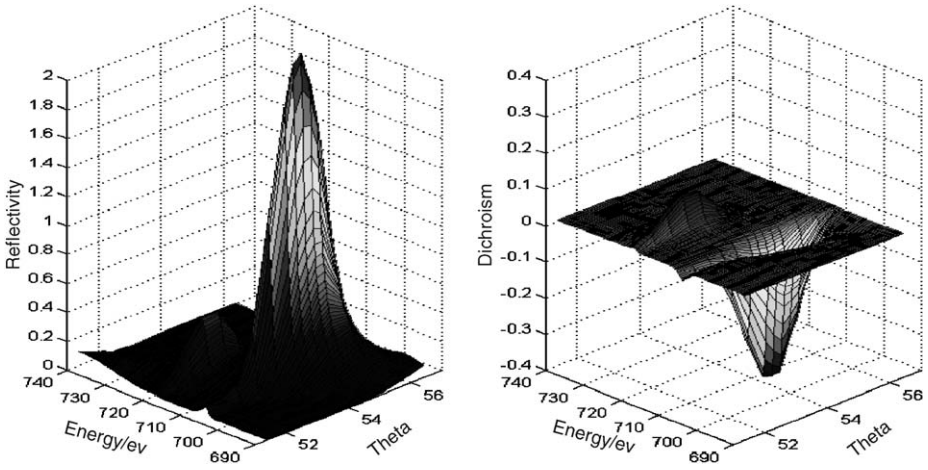

Fig. 1. Energy dispersive $\theta/2\theta$ scans near the $L_{2,3}$ Fe absorption edges around the first-order Bragg peak from $[Fe_6/Co_6]_{50}$ superlattice with period 1.08 nm: the sum (left panel) and the difference (right panel) of reflectivity for the right- and left-circular polarized radiation.

reflectivity spectra and analyze the experimental data at the $L_{2,3}$ absorption edges of Fe for the periodic multilayer $[Fe_6/Co_6]_{50}$/V, presented in Fig. 1.

2. Experimental details

A series of single crystalline BCC MgO (0 0 1)/$[Fe_x/Co_y]_{50}$ superlattices capped with 10 Å of V or Pd with individual thicknesses of Fe and Co layers varied between $x, y = 2$ and $x, y = 9$ monolayers was grown by DC magnetron sputtering [6]. The structural quality of the samples was characterized by X-ray diffraction and X-ray reflectometry with Cu K_α radiation. The main purpose of the work was the question how the magnetic moment of Co or Fe varied as a function of distance from the interface. The investigation was done by the element-specific X-ray magnetic circular dichroism measurements (XMCD) in combination with SQUID magnetometry. It has been found that the Co moment remains constant for all Fe/Co combinations studied. The Fe moment shows a complex behavior what can be attributed to the interface roughness. Anyhow an enhanced moment of 3.0 μ_B/atom was found for Fe at the Fe/Co interface.

The XMCD measurements were carried out at beamline D1011 at the Swedish synchrotron radiation facility MAX-lab. The absorption spectra were recorded through the total electron yield at different angles of incidence of the circular polarized SR beam. The samples were magnetized along the easy direction $\langle 1\,0\,0 \rangle$ in the plane of scattering. The electron yield was recorded simultaneously with the reflectivity signal.

3. Theoretical background

Calculations were performed on the basis of the general theory of reflectivity from anisotropic multilayers [7,8]. Our developed computer package XRMR is freely available at [9].

The dielectric susceptibility $\hat{\varepsilon}$ of resonant magnetic medium is a tensor:

$$\hat{\varepsilon} = 1 + \hat{\chi} = 1 + A + \mathrm{i}B\boldsymbol{h}^{\times} + C\boldsymbol{h}\cdot\boldsymbol{h}, \tag{1}$$

where $\boldsymbol{h}$ is the unit vector in the magnetization direction, $\boldsymbol{h}^{\times}$ is a tensor with components $(\boldsymbol{h}^{\times})_{il} = e_{ikl}\boldsymbol{h}_k$, where e_{ikl} is the antisymmetric Levi–Civita symbol, $\boldsymbol{h}\cdot\boldsymbol{h}$ is a diade and A, B, C are the complex functions of energy. The off-diagonal function B is responsible for the XMCD signal. In vicinity of the absorption edges, the specific energy dependencies for the circular and linear dichroism terms B and C as well as for the diagonal term A cannot be taken from the common Henke tables. Nowadays there are different methods for the measurements of the energy-dependent components of the susceptibility tensor (Faraday rotation, XMCD, XMLD, etc.). We started our calculations with the functions A, B for the Fe $L_{2,3}$ edges taken from the paper of Kortright and Kim [10]. Function C, as it was shown in Ref. [11], can be calculated as a derivative of B. It has an essentially smaller value and should be taken into account only when the influence of the off diagonal term B does not exist, e.g. in the case of the antiferromagnetic substance.

For the layered medium the Maxwell's equations are transformed to the equations for the tangential components of the magnetic $\boldsymbol{H}_t = (1 - \boldsymbol{q}\cdot\boldsymbol{q})\boldsymbol{H}$ and electric $[\boldsymbol{qE}] = \boldsymbol{q}^{\times}\boldsymbol{E}$ radiation fields:

$$\frac{\mathrm{d}}{\mathrm{d}z}\begin{pmatrix}\boldsymbol{H}_t\\ [\boldsymbol{qE}]\end{pmatrix} = ik\mathbf{M}\begin{pmatrix}\boldsymbol{H}_t\\ [\boldsymbol{qE}]\end{pmatrix}, \tag{2}$$

where the general expression for the 4×4 differential propagation matrix $\mathbf{M}$ is given in Refs. [7,8].

In L-MOKE geometry $\boldsymbol{h}$ coincides with $\boldsymbol{Y}$-axis (Fig. 2). So, the tensor $\hat{\chi}$ and corresponding propagation matrix $\mathbf{M}$

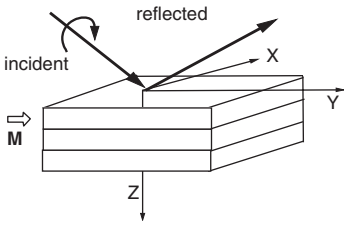

Fig. 2. L-MOKE geometry.

has the following elements:

$$\hat{\chi} = \begin{pmatrix} A & 0 & iB \\ 0 & A+C & 0 \\ -iB & 0 & A \end{pmatrix}, \tag{3}$$

$$\hat{M} = \begin{pmatrix} 0 & 0 & 1+A+C & 0 \\ \frac{iB\cos\vartheta}{1+A} & 0 & 0 & \sin^2\vartheta + A - \frac{B^2}{1+A} \\ 1 - \frac{\cos^2\vartheta}{1+A} & 0 & 0 & \frac{-iB\cos\vartheta}{1+A} \\ 0 & 1 & 0 & 0 \end{pmatrix} \tag{4}$$

with the eigenvalues $\eta_i \cong \pm\sqrt{\sin^2\theta + A \pm B\cos\vartheta}$, if we neglect C.

The solution of Eq. (2) for each layer with $\chi(z) = \text{const}$ is the matrix exponential which we calculate by means of the Silvester algorithm [12]. The integral propagation matrix of the total multilayer **L** allows us to find the 2×2 reflectivity matrix **r** for the tangential components of the magnetic radiation field $\boldsymbol{H}_t^r = \boldsymbol{r}\boldsymbol{H}_t^0$:

$$\mathbf{r} = [\gamma^d(L_1 + L_2\gamma^r) - (L_3 + L_4\gamma^r)]^- \times[(L_3 + L_4\gamma^0) - \gamma^d(L_1 + L_2\gamma^0)], \tag{5}$$

where L_i are the 2×2 blocks of the integral propagation matrix **L** and $\gamma^{0,r,d}$ are the impedance tensors [8] which determine the connection between the tangential components of the radiation field $\gamma^{0,r,d}\boldsymbol{H}_t^{0,r,d} = [\boldsymbol{q}\boldsymbol{E}^{0,r,d}]$ for the incident, reflected and transmitted waves, respectively.

4. Results and discussion

The shape of the absorption XMCD spectra is actually the energy dependency of $\mathrm{Im}(A+B)$ and $\mathrm{Im}(A-B)$ components of the susceptibility tensor. The real parts of A and B can be constructed by means of Kramers–Kroning transformation. The energy dependence of the reflectivity spectra (Figs. 1 and 3) depends on the $\mathrm{Re}(A)$, $\mathrm{Im}(A)$, $\mathrm{Re}(B)$ and $\mathrm{Im}(B)$ in much more complicated manner according to the general formalism (2) and (5). The essential variations of the shape of the reflectivity spectra measured in vicinity of the Bragg peak are also explained by the shift of the Bragg angle with the energy change, so the interference enhancement of different parts of the spectra arises at different angles.

The precise value of the Bragg peak position ϑ_B, as it was shown in Ref. [3], includes also the refraction effect. In the simplest kinematical approximation it is

$$\bar{\delta} \pm \Delta\delta = (\sin\vartheta_B - \lambda/(2D))\sin\vartheta_B, \tag{6}$$

where ϑ_B is the exact Bragg peak position, $\bar{\delta}$ is the average of the function A within the period D of multilayer, $2\delta = \mathrm{Re}\,A$, $2\Delta\delta = \mathrm{Re}\,B\cos\vartheta$. In Ref. [3] the dynamical formula was also used for the determination of the function $\mathrm{Re}(A)$, which include the small influence of the absorption $\mathrm{Im}(A)$:

$$(\delta \pm \Delta\delta)_{Fe} = (1/W)((\sin\vartheta_B - \lambda/2D) \times\sin\vartheta_B - \delta_{Co}) + \delta_{Co}, \tag{7}$$

$$W = \gamma - \frac{((\beta \pm \Delta\beta)_{Fe} - \beta_{Co})\sin^2(\pi\gamma)}{\pi^2(\gamma\beta + (1-\gamma)\beta_{Co})},$$

where $2\beta = \mathrm{Im}\,A$, $2\Delta\beta = \mathrm{Im}\,B\cos\vartheta$, γ is the relative thickness of Fe layer in the repetition period, subscripts Fe and Co refer to the optical constants of Fe and Co respectively.

We tested the both expressions for the model structure $[Fe_6/Co_6]_{50}$ with the theoretically given functions $\mathrm{Re}(A)$ and $\mathrm{Im}(A)$ [13]. The result was that the reconstructed function $\mathrm{Re}(A)$ by means of (7) agreed better with the function inserted into the calculations. So we use further the expression (7).

The experimental Bragg peak shift (or the change of the wave vector transfer $Q_B = (4\pi/\lambda)\sin\vartheta_B$) is presented in Fig. 4. The reconstructed by means of Eq. (7) function $\mathrm{Re}(A)$ is presented in Fig. 5. We see that it is quite close to the dependence obtained in Ref. [10] for the pure iron film by means of the Faraday rotation.

The Bragg angle shift gives just the average (over the repetition period) refraction of the waves in the forward and backward directions. So, this shift does not contain any new information comparing with the absorption or

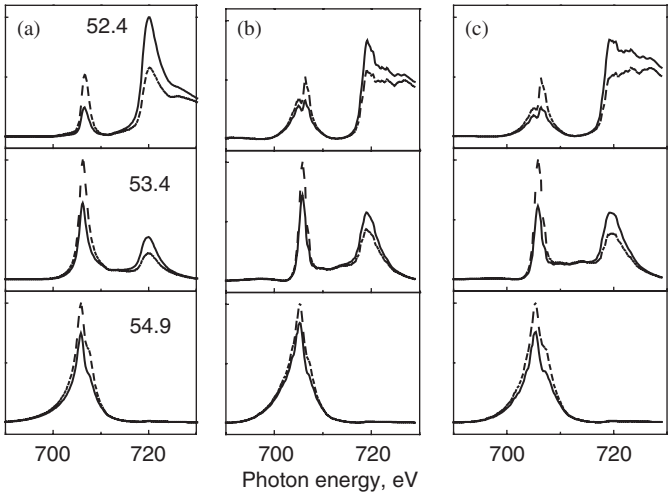

Fig. 3. Experimental (a) and theoretical spectra of the X-ray resonant Bragg reflectivity for bulk (b) and refined (c) parameters. Solid lines for the right- and dash lines for the left- circular polarizations of incident radiation. The energy range corresponds to the $L_{2,3}$ edges of Fe. The spectra are normalized. The angles are given in (a) in degrees.

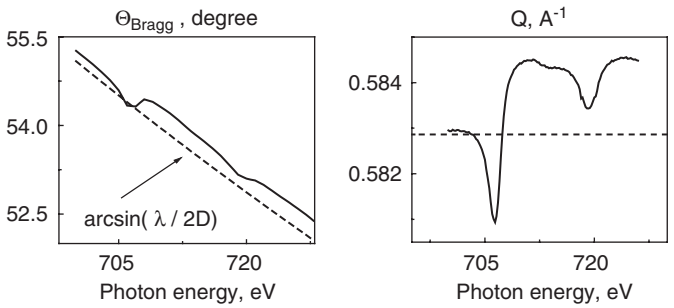

Fig. 4. Experimental angular position of the Bragg peak maximum from Fig. 1 (left) and the corresponding wave vector transfer Q (right) as functions of the photon energy. Dash lines are the simple arcsin behavior, D is the period of our superlattice.

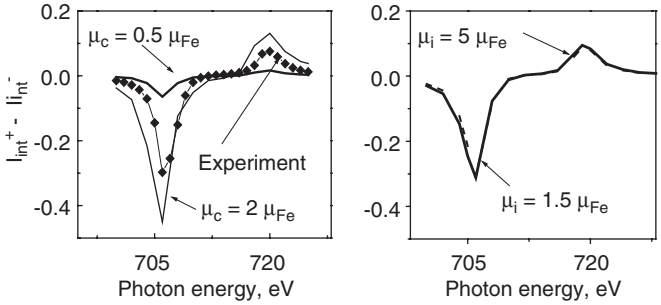

Fig. 6. Polarization difference curves of the normalized integrated intensity of the Bragg peak for the different magnetization in the central part of the iron layer μ_c (left) and in the interfaces μ_i (right). μ_{Fe} is the volume value.

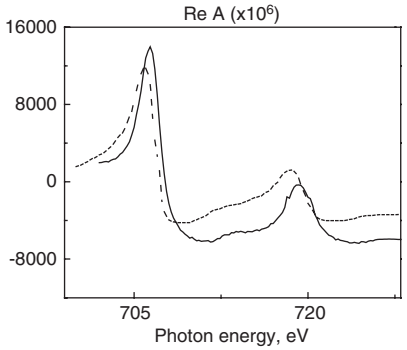

Fig. 5. The real part of the diagonal component of the susceptibility tensor, reconstructed from our experimental data (solid line) and measured in Ref. [7] by means of Faraday rotation (dash line).

Faraday rotation experiments. However, the reflectivity data possess the depth selectivity. They can give the information, which cannot be obtained by the other methods.

Here we check the influence of the magnetic moment distribution across the iron layer depth on the shape of the reflectivity spectra (Fig. 3) and on the integrated Bragg intensity (Fig. 6). The result is the first-order Bragg peak gives mainly the information about the magnetic moments in the center of Fe layers.

By comparison of our calculations with the experimental dependencies we have found the value of the magnetic moment of Fe in the center of iron layers which occurs equal to 2.60 ($\pm$0.04) μ_B/atom.

5. Conclusions

Our analysis of the reflectivity spectra for the sample $[Fe_6/Co_6]_{50}$ reveals the enhancement of the Fe magnetic moment in the central part of iron layers. So we can conclude that the larger value of Fe average magnetic moment for that sample determined in Ref. [6] by SQUID magnetometry (2.9 μ_B) and XMCD (2.74 μ_B) can be explained not only by the enhancement of the interface magnetic moment of Fe.

Acknowledgement

We acknowledge the financial support from Uppsala University, RFBR (05-02-16770) and INTAS (01 0822).

References

[1] J.B. Kortright, D.D. Awschalom, J. Stöhr, S.D. Bader, Y.U. Idzerda, S.S.P. Parkin, I.K. Schuller, H.-C. Siegmann, J. Magn. Magn. Mater. 207 (1999) 7.
[2] H.-Ch. Mertins, S. Valencia, A. Gaupp, W. Gudat, P.M. Oppeneer, C.M. Schneider, Appl. Phys. A 80 (2005) 1011.
[3] M. Sacchi, C.F. Hague, L. Pasquali, A. Mirone, J.-M. Mariot, P. Isberg, E.M. Gullikson, J.H. Underwood, Phys. Rev. Lett. 81 (1998) 1521.
[4] P. Carra, B.T. Thole, M. Altarelly, X. Wang, Phys. Rev. Lett. 70 (1993) 6689.
[5] L. Séve, N. Jaouen, J.M. Tonnerre, D. Raoux, F. Bartolomé, M. Arend, W. Felsch, A. Rogalev, J. Goulon, C. Gautier, J.F. Bérar, Phys. Rev. B 60 (1999) 9662.
[6] M. Björck, G. Andersson, B. Lindgren, R. Wäppling, V. Stanciu, P. Nordblad, J. Magn. Magn. Mater. 284 (2004) 273.
[7] R.M. Azzam, N.M. Bashara, Ellipsometry and Polarized Light, North-Holland Publishing Company, Amsterdam, New York, London, 1977.
[8] G.N. Borzdov, L.M. Barkovskii, V.I. Lavrukovich, Zh. Priklad. Spectrosk. 25 (1976) 526.
[9] http://solst.phys.msu.su/andreeva/index.html.
[10] J.B. Kortright, S.-K. Kim, Phys. Rev. B 62 (2000) 12216.
[11] J. Kunes, P.M. Oppeneer, Phys. Rev. B 67 (2003) 024431.
[12] A. Ango, Complements de mathematiques, Paris, 1957.
[13] M.A. Andreeva, A.G. Smekhova, Izv. RAN Ser. Fiz. 69 (2) (2005) 259.